IEEE Access
Multidisciplinary ⋮ Rapid Review ⋮ Open Access Journal

Received 31 July 2024, accepted 19 August 2024, date of publication 23 August 2024, date of current version 3 September 2024.

Digital Object Identifier 10.1109/ACCESS.2024.3448507

RESEARCH ARTICLE

Redundant Configuration and Fault Tolerance Control Method for Enhanced Reliability of Energy Storage System

IN-HO CHO[1], (Member, IEEE), SEONG-YUN PARK[2], BEOM-JUN KIM[1], AND JONG-HOON KIM[2], (Senior Member, IEEE)

[1]Department of Electronic Engineering, Korea National University of Transportation, Chungju-si, Chungbuk 27469, Republic of Korea
[2]Department of Electrical Engineering, Chungnam National University, Daejeon 34134, Republic of Korea

Corresponding author: In-Ho Cho (ihcho@ut.ac.kr)

This work was supported by the National Research Foundation of Korea (NRF) through Korean Government (MSIT) under Grant RS-2023-00210755.

ABSTRACT The use of energy storage systems (ESSs) is increasing in the industry as part of global efforts to reduce carbon emissions. In particular, large-capacity ESSs that adopt lithium-ion batteries, which have high energy density characteristics, are being used not only in stationary applications but also in mobility industry fields such as vehicles and ships. However, ESSs with lithium-ion batteries have a high risk of fire and failure, which reduces the reliability of the system. This paper studies the redundant type ESS configuration and its fault tolerance control method for enhanced reliability of ESSs to which lithium-ion batteries are applied. Hence, we present a new control method for improving the cycle life of ESSs. The effectiveness of the proposed control method is validated using a 10S-1P configuration lithium-ion battery module, with reference to the operating profile of railway vehicles.

INDEX TERMS ESS, redundant, reliability, railway vehicles.

I. INTRODUCTION

The recent increase in global carbon emission reduction regulations has driven the industry to reduce fossil energy use, which is the main driving force behind the growth of the energy storage system (ESS) market 21]. The automobile industry is reducing the production of internal combustion engine cars and increasing the production of electric vehicles adopting ESSs with lithium-ion batteries in order to reduce fossil fuel usage and increase energy efficiency [2], [3]. Power grid applications also use an operating method that uses large ESSs to store electricity at late-night hours when power demand is relatively low, and the energy is stored for daytime use when power consumption is high [4]. This is an effective method to reduce energy consumption by limiting the size of peak power generation in the power plant. The application of large-capacity ESSs is essential in the renewable energy generation system to compensate for the limitations of new renewable energy with irregular power generation characteristics. Recently, electric railway transportation, which previously received propulsion power through a catenary, is also being developed in the direction of mounting a large-capacity ESS to increase the use of regenerative energy [5].

Thus, the field of ESS utilization is expanding, and at the same time, the capacity of the ESS applied to each industry is rapidly increasing [6]. The increased capacity of the ESS can increase the power supply stability and efficiency of the system to which the ESS is applied, but as the number of lithium-ion batteries constituting the ESS increases, the risk of fire or failure of the system increases [7]. Therefore, research on failure prevention technology is drawing much attention these days because it can enable the ESS to continue to operate even in the event of a failure of constituent parts of

The associate editor coordinating the review of this manuscript and approving it for publication was K. Srinivas.

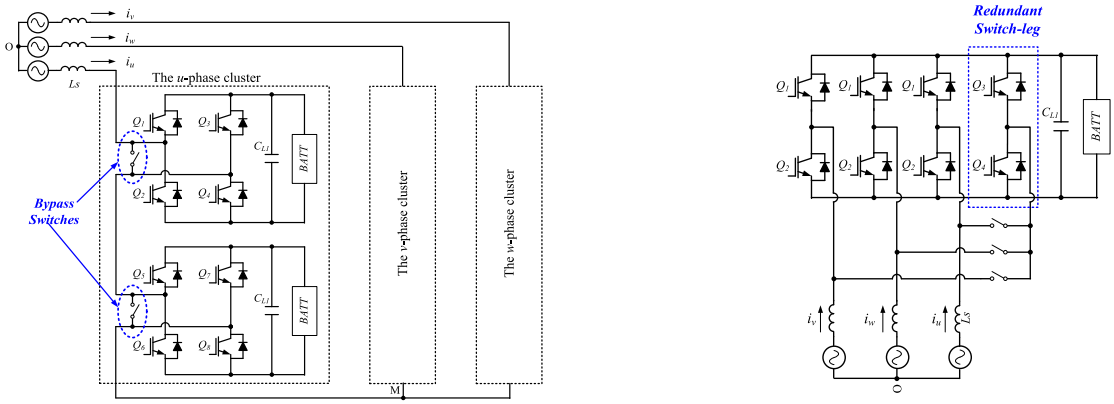

(a) Bypassing a fault converter scheme

(b) Parallel redundancy leg scheme

FIGURE 1. Redundant technology for power conversion circuit [9], [10].

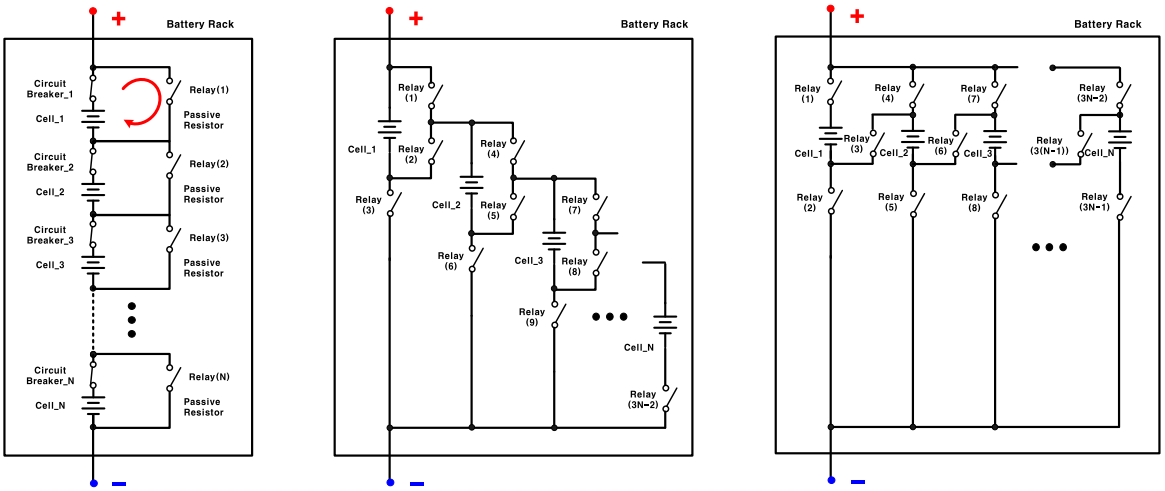

(a) Parallel switch type_1

(b) Parallel switch type_2

(c) Parallel switch type_3

FIGURE 2. Fault-reconfiguration method for battery modules [14].

the ESS, such as a lithium-ion battery cell, a battery module, or a power converter.

One of the failure prevention technologies for the ESS is a circuit and control method that can respond to a failure in the power converter of the ESS. In that research, they additionally configured switches that create a bypass path through which current can flow while blocking the connection of faulty parts in the event of a failure, as shown in Fig. 1. That method is based on the assumption that among the components of the converter, short-life-cycle elements, such as capacitors easily cause failure. By reconfiguring the circuit in this way, the ESS can continuously supply the output power even in the event of a failure. However, there are some limitations to that method. First, in order for the reconfigured ESS to operate at the rated output power even after a failure, individual power converters must be designed with a larger voltage/current margin at the time of initial design. Second, in general, a lithium-ion battery is chosen as the component which has the shortest life-cycle in the ESS. That means that the conventional bypass method has a limitation in practical utility [8], [9], [10], [11].

A number of studies have been conducted on circuit technology, as shown in Fig. 2; the control method configures a new battery pack connection by excluding the failed module and using only the remaining battery modules in the event of a battery module failure. The simplest method among those proposed research is additionally configures a series switch and a parallel switch in an individual battery module [11], [12], [13], [14]. This method opens the serial switch connected to the corresponding module to block the flow of current to the module and closes the parallel switch to bypass the current of the battery pack when a failure module occurs.

This method has the advantage of simple control, but the circuit configuration requires a number of additional switches, and the output voltage of the ESS decreases when the ESS is operated after bypassing the failure module. In order to improve these disadvantages, a number of studies

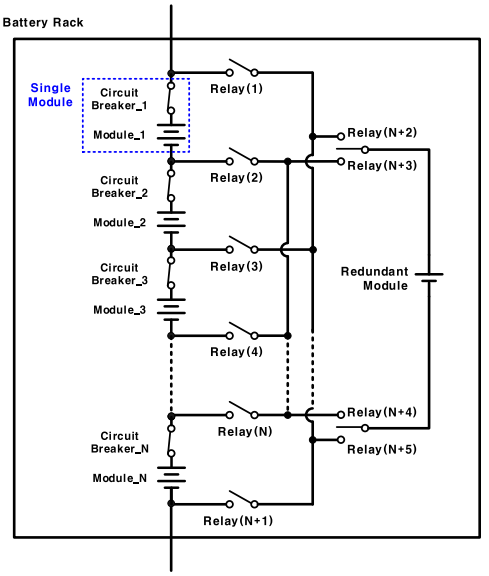

FIGURE 3. Circuit configuration of battery rack with redundant characteristic [17].

have been conducted to reduce the number of additionally used switches [15], [16]. However, even with a simplified circuit configuration method, there is still a disadvantage: The the battery pack voltage decreases due to a decrease in the number of battery modules connected in series, which causes a decrease in the capacity of the ESS.

This paper reviews the battery rack/module configuration methods that allow the ESS to operate normally without reducing voltage when a battery module fails. In addition, we propose a control method that considers the life of the reconfigured ESS. We analyzed the circuit configuration and operation mode of the proposed method and experimentally verified the effect of improving the life expectancy of the ESS that can be obtained through the proposed control method using a small-scaled battery cell/module. In particular, design guidelines are presented and their validity is verified for railway vehicle applications, which have recently been actively reviewed for application of large-capacity battery systems. The results show that the proposed method can effectively improve the life expectancy of ESSs by preventing the overcharging and over-discharging of battery modules.

II. BASIC OPERATION OF THE REDUNDANT TYPE MODULE CONFIGURATION

Fig. 3 shows the circuit configuration of an ESS with redundant characteristics [17]. This circuit has a configuration that adds one redundant module to replace the failed battery module in the existing battery rack configuration in which 'N' battery modules are connected in series. This system has the advantage that the redundant module can replace any module among the series configuration modules through connection switch control, while the number of added modules is minimized. All relay switches, which are from 'Relay(1)' to 'Relay(N+1)', are open in normal operating conditions

TABLE 1. Switches operation for the reconfiguration.

Fault Module	Module_1	Module_2	Module_3	…	Module_N
Relay(1)	Closed	Open	Open	…	Open
Relay(1)	Closed	Closed	Open	…	Open
Relay(1)		Closed	Closed	…	Open
Relay(1)			Closed	…	Open
…	…	…	…	…	…
Relay(N)	Open	Open	Open	…	Open
Relay(N+1)	Open	Open	Open	…	Open
Relay(N+2)	Closed	Open	Closed	…	Closed
Relay(N+3)	Open	Closed	Open	…	Open
Relay(N+4)	Closed	Open	Closed	…	Closed
Relay(N+5)	Open	Closed	Open	…	Open

where there is no failure of the battery module. If a failure is detected in a specific module among the serially configured modules, a redundant module replaces the failed module through relay switch control. When a failure occurs in 'Module_1', the circuit breaker connected to the module is opened to isolate the failed battery module. Afterwards, the adjacent relay switches, 'Relay(1)' and 'Relay(2)', are closed, and the path of the current previously entering 'Module_1' is bypassed so that it can be connected to the redundant module. Table 1 shows the relay switches operation for reconfiguration of a battery rack composed of 'N' serial modules. Fig. 4 (a) and Fig. 4 (b) show the circuit connection when a failure occurs in 'Module_1' and 'Module_2', respectively. This configuration mechanism can be applied to the module level configuration.

III. CONCEPT OF THE PROPOSED CONTROL METHOD

In the reconfiguration circuit shown in Fig. 4, the failed battery module is replaced with a redundant module. This circuit configuration method can be applied equally to modules composed of a series connection of battery cells. The lifespan of lithium-based batteries, which are currently widely used as large-capacity energy storage devices, is divided into cycle life and calendar life. In the case of ESSs, the cycle life is a more important factor in determining the overall lifespan of the system [18]. This is because ESSs are often subjected to frequent charging and discharging operations. As a result, even after a failed battery module is replaced, the overall lifespan of the ESS is still limited by the remaining cycle life of the battery cells and modules that have already been used. Therefore, even if the ESS has reached its end of life, the newly added redundant module may still have some remaining life. However, the overall performance of the ESS will be reduced, as the redundant module will not be able to fully compensate for the reduced capacity of the other modules.

This paper proposes a control method that improves the lifespan of the entire ESS while fully utilizing the expected lifespan of all battery modules in the ESS configuration

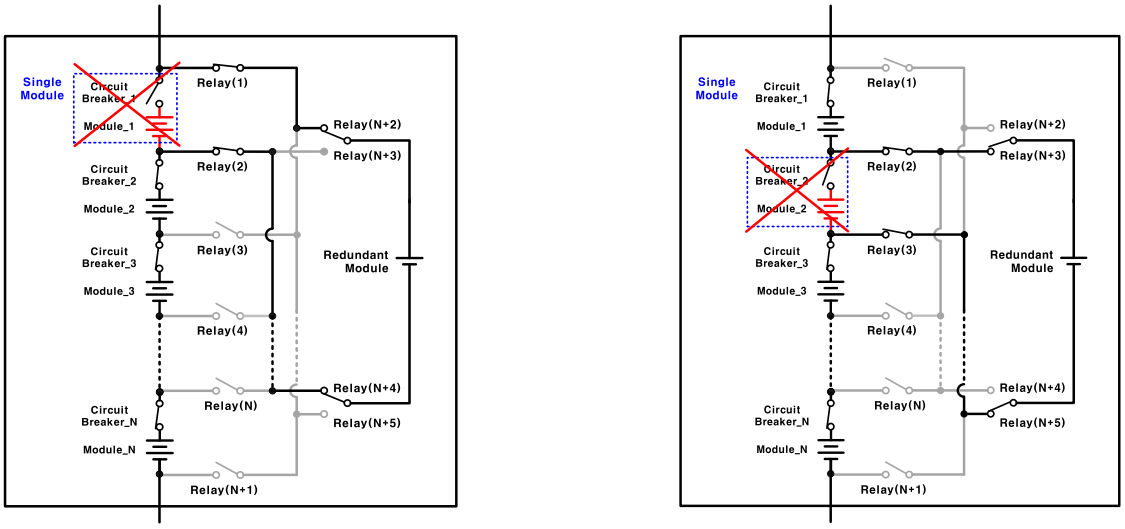

(a) Module_1 fault condition

(b) Module_2 fault condition

FIGURE 4. Operation of the circuit in fault state.

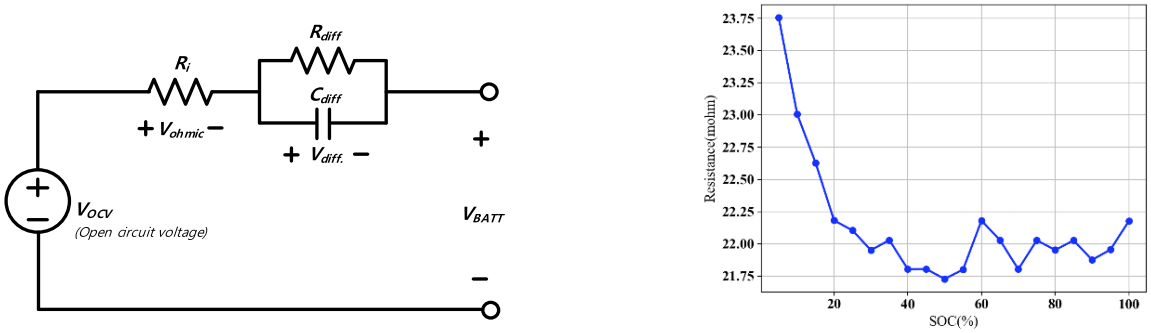

(a) Equivalent circuit of a Li-ion battery

(b) Battery internal resistance on the SOC level

FIGURE 5. Equivalent circuit model and internal resistance value of the Li-ion battery.

with redundant characteristics. In particular, the depth of discharge (DOD), which is the ratio of battery capacity that is frequently used in charge/discharge operations to the total battery capacity, and the normal state of charge (SOC) level, which is associated with the cell voltage level under normal operating conditions, are the two main design factors in the proposed control method. For the circuit shown in Fig. 3, in the battery rack configuration where the battery modules are connected in series, the current entering the battery rack flows equally through all battery modules, so the magnitude of current entering individual battery modules cannot be different. Therefore, the control for changing the DOD level has limitations for application, and what is needed is a control method that extends the lifespan of the ESS by differentiating the nominal SOC level.

Fig. 5 shows the internal resistance values according to the SOC level of the high-capacity lithium-ion cell (INR-18650 29E) obtained using the equivalent circuit model of the battery and the hybrid pulse power characterization (HPPC) method. As shown in the figure, lithium-based batteries are characterized by different internal resistance values depending on the SOC level [19]. This resistance causes power loss during charging and discharging of the battery that has a direct correlation with heat generation of the battery. In the case of a battery that stores and releases energy through chemical reactions, the rate of chemical reactions varies depending on the temperature. An excessive chemical reaction rate is the cause of accelerating the aging of the battery [20], [21]. The results of this study show that it is possible to control the lifespan of individual battery modules by controlling the power loss of each battery module. According to the Arrhenius equation (1), which shows the correlation between the rate of chemical reaction and the temperature, the rate of chemical reaction has a logarithmic linear relationship with the temperature, which means that the lifespan of the battery is affected by the operating temperature of the battery. Therefore, it is possible to apply a control method that extends the lifespan of an ESS by controlling the amount of heat generated by each battery cell/module.

$$r = A \times e^{\left(\frac{E_a}{kT}\right)} \tag{1}$$

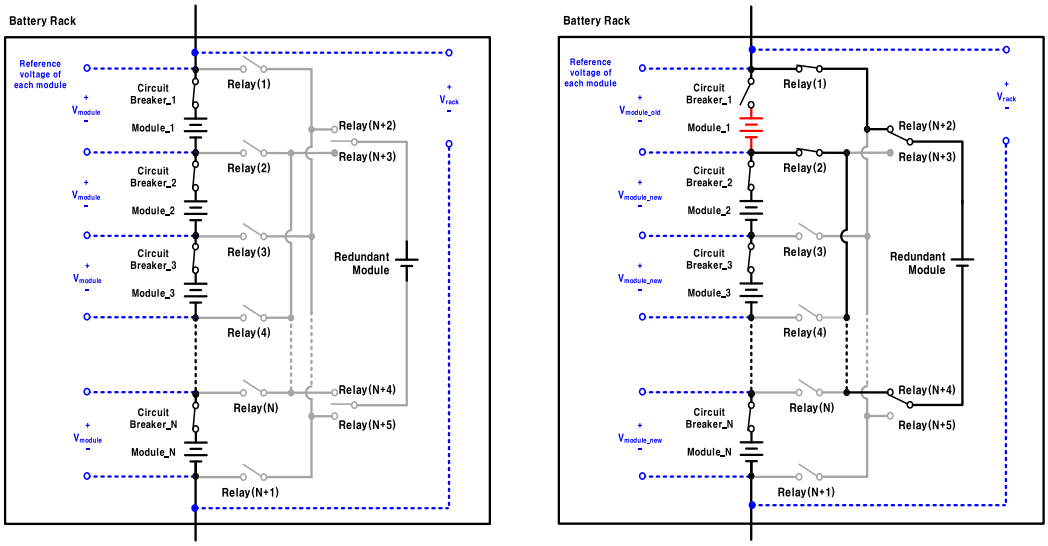

(a) Conventional operating condition

(b) Redundant applied operating condition

FIGURE 6. Operation of the proposed control method.

where r is the reaction rate, k is Boltzmann's constant, A is the frequency factor, E_a is the activation energy, and T is the absolute temperature.

IV. CONTROL METHOD FOR MAXIMIZING THE LIFETIME OF AN ESS

In a battery rack composed of series-connected battery modules, the link voltage, which is the voltage of the battery rack, is determined by the sum of the voltages of the battery modules connected in series. Therefore, even with a control method that changes the nominal SOC of each battery module, the overall link voltage must be maintained. Under this operating condition, the aging rate of a battery module that is continuously being used can be slowed down by reducing the internal power loss of the module after the redundant module is applied. That means the module needs to operate under the nominal SOC level with the lowest internal resistance value. The link voltage should be compensated through modulating the control voltage of the redundant module. Fig. 6 shows an example of applying the proposed control method.

In the conventional control method, the nominal voltage of the battery module is determined by dividing the voltage of the battery rack by the number of battery modules configured in series. The voltage value obtained through equation (2) is applied as the same control command to all battery modules. On the other hand, in the proposed control method, the voltages of the battery module and the newly adopted battery module, which is called redundant battery module, are controlled differently. In conventional modules, the nominal SOC level at which the battery resistance is minimized is selected, and the control voltage of the redundant battery module is determined according to Equations (3) and (4). In Equations (3) and (4), 'N' is the number of modules connected in series, and 'α' represents the difference between the initially set nominal SOC voltage (V_{module}) and the battery module voltage at the SOC where the resistance of the battery cell is minimized.

- Nominal voltage for battery module in conventional method

$$V_{module} = V_{pack} \div N \tag{2}$$

- Nominal voltage for battery module in proposed method

$$V_{module\_old} = V_{module} - \alpha \tag{3}$$

- Nominal voltage for battery module in proposed method

$$V_{module\_new} = V_{module} + \alpha \times (N - 1) \tag{4}$$

V. DESIGN CONSIDERATIONS OF THE PROPOSED CONTROL METHOD

The proposed control method adjusts the control voltage levels of individual battery modules after the detection of a battery fault. The control voltage of the module that has been in continuous use, V_{module_old}, is adjusted to correspond to the SOC level that minimizes internal resistance. A newly added battery module, the redundant battery module, compensates for the link voltage level. In this process, the difference between the previous control voltage level of V_{module_old} and the altered control voltage level is α. Under ideal conditions, the magnitude of α can be freely designed. However, in practical applications, the design range is constrained based on the usage patterns of batteries specific to each application. For example, in electric vehicles, where full charging and deep discharging conditions are frequently represented, the design range of α is limited.

Generally, lithium-ion batteries have the lowest internal resistance in the mid-range SOC region as in Fig. 5 (b).

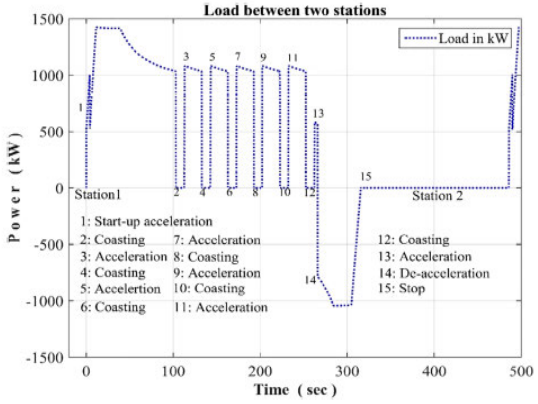

(a) 1-cycle pattern

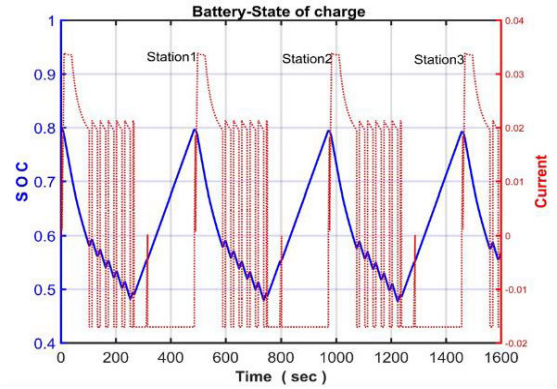

(b) N-cycle pattern

FIGURE 7. Operating pattern of an ESS in a fuel-cell hybrid railway propulsion system.

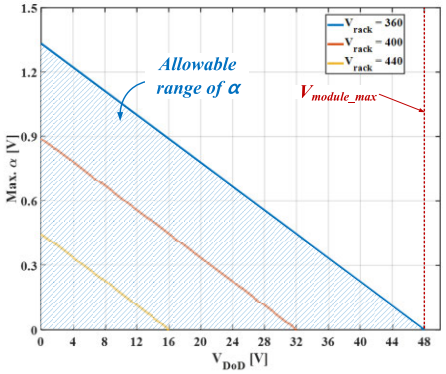

FIGURE 8. Allowable design range of α in the proposed control method.

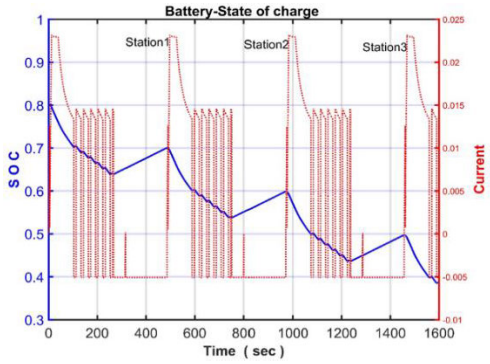

FIGURE 9. Operating pattern of an ESS in a tram propulsion system.

Considering the characteristic that the internal resistance of a battery is the lowest in the SOC 40∼50% region, setting the voltage level at SOC 50% as the nominal voltage results in a battery rack with an energy swing range of +/- 50% based on SOC 50%. Therefore, it is effective to set the nominal voltage based on SOC 50% in applications with frequent charge/discharge operation. However, if the operational pattern involves only discharge operations after a single full charge, the usable battery capacity can decrease to 50% of its rated capacity when the nominal voltage set to a SOC 50% level. Therefore, the design of α needs to consider not only battery lifespan but also usage patterns. We propose an optimal design method for each of the following two cases: (1) a battery operation pattern that maintains a consistent normal SOC level through repeated charge / discharge cycles, and (2) a usage pattern that continuously shows discharge operations after a single charge, which results in a gradual decline of the normal SOC level.

A. CASE 1—SUSTAINING A CONSISTENT NOMINAL SOC LEVEL

It is not difficult to find an application that maintains a normal SOC level among applications that use large capacity ESS. In renewable energy generation systems using solar and wind power, industrial ESSs that compensate for the unevenness of power generation show similar usage patterns. In addition, in the railway sector, a large-capacity ESS is used to supply stable power to the motor load during propulsion operation and store regenerative energy during braking in a propulsion system using renewable energy as power. Fig. 7 shows the ESS operation pattern in the fuel cell hybrid railway vehicle propulsion system [22], [23]. The dotted line represents charge/discharging current and the solid line shows the SOC level of the ESS in Fig. 7. The ESS applied to these applications shows that the charge and discharge are repeatedly manifested in a situation where the SOC is maintained at a certain level. The ESS applied to these applications is characterized by a cyclic charge and discharge pattern while a steady nominal SOC level is maintained.

The nominal SOC level of the modules that operate continuously needs to be changed to the intermediate range where internal resistance is minimized for improving the cycle life. However, the nominal SOC level of the newly configured module V_{module_new} is affected by the nominal voltage of other battery modules V_{module_old} for link voltage compensation as shown in (4). Equation (5) defines the design range of α. It is assumed that the magnitude of the SOC change during battery charge/discharge is uniform, and V_{module_new} is assumed to be greater than V_{module_old}.

V_{DOD} represents the voltage variation based on DOD, V_{rack} represents the total rack voltage, and V_{module_max} indicates the maximum voltage capacity of the module.

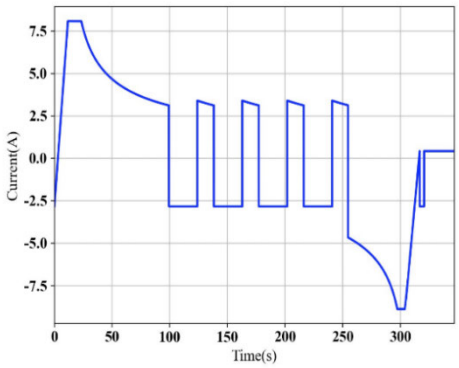

FIGURE 10. Cycle profile for aging test.

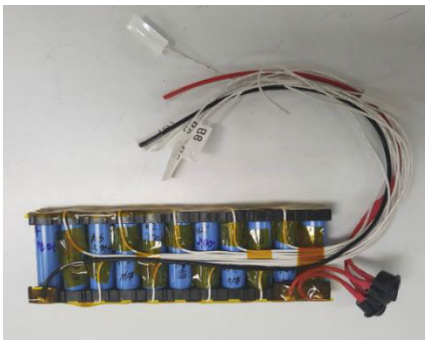

FIGURE 11. The proposed type battery module with a redundant cell.

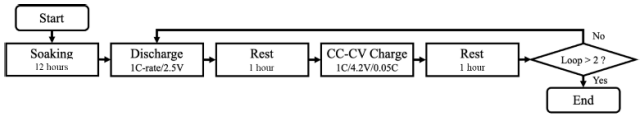

FIGURE 12. Experimental procedure for cell capacity scanning test.

Fig. 8 provides a schematic representation of this concept. As depicted in Fig. 8, the available range of α diminishes as DOD increases, serving as a constraint on setting the nominal SOC level for an enhanced lifespan.

- Allowable design range of α,

$$V_{module\_old} < V_{module\_new} \leq (V_{module\_max} - \frac{V_{DOD}}{2})$$
$$\rightarrow 0 < \alpha[V] \leq \frac{V_{module\_max}}{N-1} - \frac{V_{rack}}{N(N-1)} - \frac{V_{DOD}}{2(N-1)} \quad (5)$$

B. CASE 2–DECREASING A NOMINAL SOC LEVEL

In battery-powered trams, the ESS is fully charged at the train depot, and the energy stored in the ESS is utilized for operation throughout the entire operating cycle without requiring extra charging until the end of the operating period. Consequently, the ESS adopted in tram vehicles need to be designed differently from the ESS designed with 'Case 1' scenario. Since the SOC level decreases proportionally to the vehicle's operating time, the planned total route length

TABLE 2. 18650-29E cell specification.

	Nominal capacity	Charging Voltage	Nominal Voltage	Discharge Cut-off Voltage	Charging Current
Value	2,850mAh	4.20V	3.65V	2.50V	1,375mA

TABLE 3. Initial capacity experiment of the cells.

10S-1P						
Cell NO.	1	2	3	4	5	
Capacity (Ah)	2.7780	2.7790	2.7685	2.7747	2.7731	
Cell NO.	6	7	8	9	10	
Capacity (Ah)	2.7565	2.7750	2.7763	2.7716	2.7839	
11S-1P						
Cell NO.	1	2	3	4	5	6
Capacity (Ah)	2.7741	2.7759	2.7771	2.7706	2.7604	2.7762
Cell NO.	7	8	9	10	11	
Capacity (Ah)	2.7793	2.7748	2.7721	2.7806	2.7689	

becomes an important factor when designing the capacity of the ESS. Fig. 9 shows an example of ESS operational patterns in tram vehicles. The nominal SOC level of the ESS, which is represented by the solid line in Fig. 9, decreases proportionally to the vehicle's operating time. The operational profile in Fig. 9 is organized by removing the amount of power supplied through fuel cells from the operation profile of the FC-hybrid propulsion system shown in Fig. 7. For 'Case 2' as well, the design of the control variation range 'α' follows equation (5), similarly to 'Case 1.' However, in most scenarios where such operational patterns are applied, the DOD of the battery is designed to be maximized to minimize the volume and weight occupied by the battery pack, thereby utilizing the available battery capacity to the fullest extent possible. As can be seen in Fig. 8, the control variation range 'α' diminishes significantly as the magnitude of DOD increases, and the application of the control voltage variation method is limited.

VI. EXPERIMENTAL VERIFICATION

To verify the effect of the proposed reconfiguration ESS control method on the ESS lifetime increase, a battery module prototype was fabricated and a charging/discharging cycle experiment of 14,000 cycles was conducted using the hydrogen fuel cell hybrid railway vehicle operating pattern shown in Fig. 10. This experiment applied the voltage setting method at the cell level, which was previously analyzed, instead of the voltage setting method at the module level. In the experiment, two types of battery module prototypes with 10Series-1Parallel cell configurations, the conventional type and the proposed type, were fabricated and the experiment was conducted. The conventional type was fabricated using 10 cells to make a 10S-1P prototype, and the proposed type was composed of 11 cells including 1 redundant cell. The proposed type module includes a relay that changes the circuit connection configuration along with the redundant cell. A photograph of the proposed type used in the experiment is shown in Fig. 11. In the conventional prototype, all serially

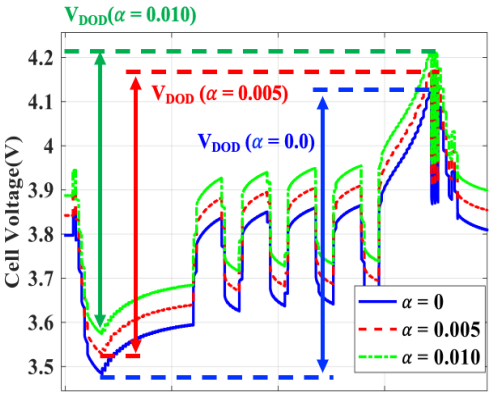

FIGURE 13. Voltage variation of the redundant cell upon the design range α.

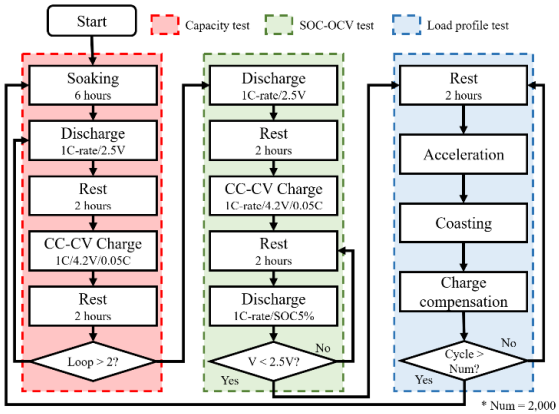

FIGURE 14. Reference performance test procedure.

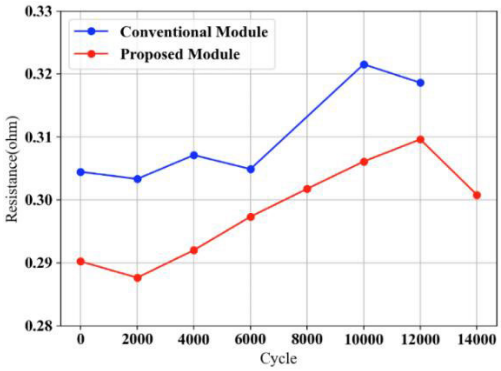

FIGURE 15. Cycle test result - Cell resistance trends [24].

configured cells were designed to operate with the same cell control voltage, the nominal voltage. In the proposed type, the experiment was conducted under the same conditions as the conventional prototype up to 10,000 cycles. At the 10,000-cycle point, the circuit was reconfigured to use the redundant cell. After the circuit reconfiguration, the control voltage of the newly applied redundant cell and the cell that was used since the beginning were designed to be different.

The experiment used a high-capacity type of lithium-ion battery cell model, Samsung SDI 18650-29E. The basic specifications of the battery cells used in the experiment are listed in Table 2. In addition, to improve the reliability of the experimental results, we conducted an initial capacity experiment of the cells (see Fig. 12), and selected cells with a cell-to-cell capacity deviation of less than 1×10^{-6} to form the prototype module as shown in [Table 3].

In order to properly select the "design range α" applied to the redundant cell, it was necessary to know the voltage variation range V_{DOD} during a single charge/discharge cycle. We used the equivalent circuit model of the lithium-ion battery to estimate the terminal voltage fluctuation range of the cell. The equivalent circuit was constructed using the 1st-order RC ladder equivalent circuit model of Fig. 5 (a) and the internal parameter values of the INR-18650 29E cylindrical cell were applied. The terminal voltage change of the cell was simulated by applying the railway vehicle load profile. Fig. 13 shows the results of the terminal voltage change according to the design range variation. In Fig. 13, the case where the design range α is 0 is a graph showing the case where the nominal SOC level of the battery cell that has been used since the beginning of the cycle and the newly applied redundant cell are the same. The nominal voltage in this case is 3.79V. As the α value increases, the nominal voltage of the redundant cell is set higher than 3.79V, and the nominal voltage of the cells that have been used so far is set lower than 3.79V.

When the railway vehicle load profile is applied with $\alpha = 0$, the maximum cell voltage reaches about 4.11V as shown in Fig. 13. When $\alpha = 0.005$, the maximum charging voltage reaches 4.17V, and when $\alpha = 0.01$, the maximum charging voltage reaches 4.21V. Since the maximum charging voltage of the INR-18650 29E cell is 4.2V as specified by the manufacturer, V_{cell_max} should not exceed 4.2V. Therefore, α needs to be designed to be less than 0.01 in order to not exceed the maximum allowable voltage condition of the cell. In this experiment, the maximum operating voltage condition of the cell was set to 4.17V considering the safety margin. As a result, α was designed to be 0.005 to improve the lifetime of the reconfigured battery module, and the nominal voltage of the redundant cell was selected as 3.835V and the nominal voltage of the existing cell was selected as 3.785V.

To verify the change in lifetime characteristics between the proposed module, which applies the proposed lifetime improvement control method, and the conventional module, which is controlled to operate with all cells with the same nominal voltage, a total of 14,000 cycle tests were performed to compare the aging trends. A reference performance test was performed every 2,000 cycles to confirm the change in cell capacity. The cycle test procedure is composed of three main steps: capacity test, SOC-OCV test, and load profile test. This is also called as reference performance test (RPT), and the detailed test procedure is shown in Fig. 14.

In the capacity test, a 6-hour soaking time was allowed to stabilize the internal chemical structure of the cell, and

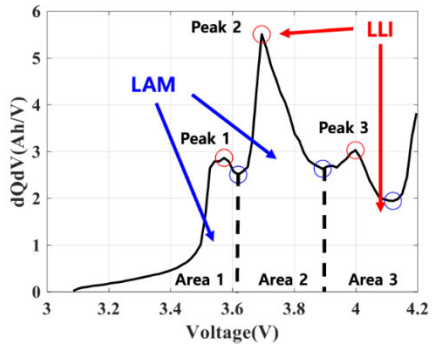

FIGURE 16. Aging analysis using IC curve [25].

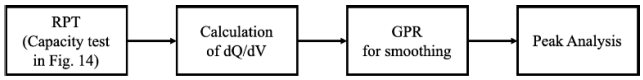

FIGURE 17. The process of battery aging evaluation by Incremental capacity analysis (ICA) with Gaussian process regression (GPR).

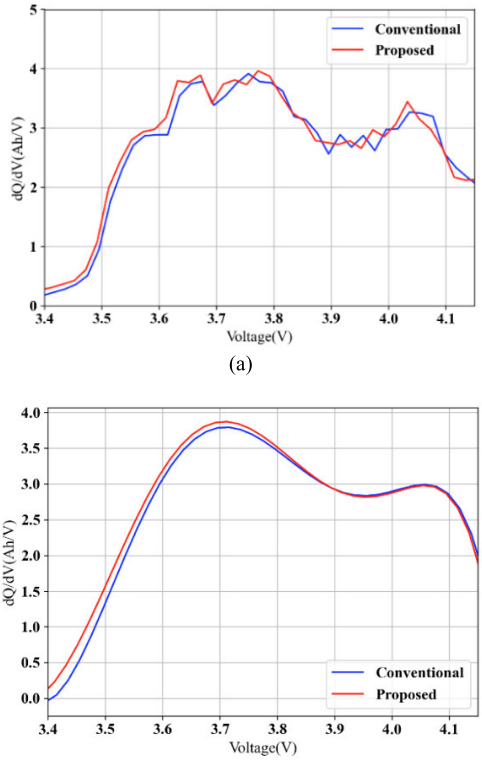

FIGURE 18. IC curve of Cell #10; (a) Without noise filter (b) Eliminating noise using GPR.

the experiment was conducted through the following steps: 1C-rate discharge to the cut-off voltage / 2 hours of rest time / 1C-rate full charging / rest. After that, the OCV level was determined by lowering the SOC level by 5% at a 1C-rate discharge current to compensate for the change in the SOC-OCV table due to aging. After the SOC-OCV test, a 2,000-cycle aging test was performed again using the load profile.

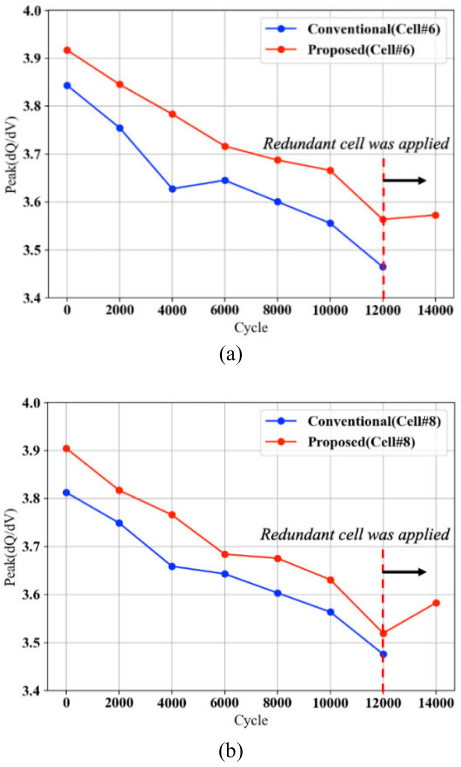

FIGURE 19. The comparison of decreasing ICA peak with cycle between conventional module and proposed module; Cell #6 (a) & Cell #8 (b).

Fig. 15 shows the results of the capacity and resistance value changes over the course of the cycling test. As can be seen from the experimental results, both the conventional and proposed modules exhibited a trend of capacity loss and resistance increase. Notably, the resistance of the proposed module decreased after the control method was changed at the 12,000-cycle point.

To provide a clearer comparison of the aging test results, the incremental capacity analysis (ICA) method, which analyzes the electrochemical characteristics of batteries based on electrical signals of voltage/current, was additionally applied. ICA can be represented as follows by expressing the current capacity in voltage within a certain voltage range.

$$\frac{dQ}{dV}_n = \frac{Q_n - Q_{n+1}}{V_n - V_{n+1}} \frac{V_{DOD}}{2(N-1)} \tag{6}$$

The aging status of the battery can be classified into three categories: (1) conductivity loss (CL), (2) loss of active material (LAM), and (3) loss of lithium inventory (LLI) [25].

(1) Conductivity loss is mainly caused by the loss of the collector, and since it tends to increase the resistance, the analysis curve tends to move to the right or left depending on the charging/discharging operation.

(2) The decrease in active material is mainly caused by the decomposition of the electrolyte, and it causes a decrease in capacity or an increase in resistance. This changes the analysis curve in the direction of decreasing the area of the curve.

TABLE 4. The average of ICA peak heights between conventional module and proposed module.

Peak of ICA (dQ/dV)	Conventional module	Proposed module
0	3.78	3.90
2000	3.68 (-0.10)	3.81 (-0.09)
4000	3.63 (-0.05)	3.75 (-0.06)
6000	3.59 (-0.04)	3.68 (-0.07)
8000	3.54 (-0.05)	3.62 (-0.06)
10000	3.50 (-0.04)	3.60 (-0.02)
12000	3.42 (-0.08)	3.48 (-0.12)
14000	-	3.81 (+0.33)

(3) The decrease in lithium inventory is caused by the collapse of the crystal structure and the dissolution of transition metals, and it mainly affects the decrease in the peak of the curve.

In this study, we conducted an ICA analysis using a 1C-rate charging/discharging current and a 20mV voltage deviation, as shown in Figure 16. In addition, a noise filtering method such as Gaussian process regressor (GPR) was applied to remove noise from the analysis results. The ICA experiment and analysis procedure are shown in Fig. 17. Fig. 18 shows the IC curves before and after applying GPR. Fig. 19 shows the results of analyzing the peak values of the ICA curves obtained from the experiment. As can be seen in Fig. 19, when the proposed method was applied at 12,000 cycles, the slope of the decrease in the peak value size changed. Since the decrease in the peak value size indicates the aging of the cell, the analysis results confirmed that the aging tendency decreases when the proposed method is applied.

In the aging cycle test, the ICA peak value was measured every 2000 cycles. Table 4 shows the average peak values of individual cells in the conventional module and the proposed module. The values in parentheses in Table 4 show the change in the ICA peak value after each 2,000-cycle aging test. As shown in the experimental results, the ICA peak values of both the conventional module and the proposed module decreased by a similar amount (0.04∼0.07 Ah/V) every 2,000 cycles until 12,000 cycles. However, the proposed module, which underwent additional testing for 2,000 cycles after applying the redundant cell configuration method and the control method that changed the nominal voltage at 12,000 cycles, showed an increase in the ICA peak height value at 14,000 cycles. This increase was due to the proposed module's cells operating in an area with low internal resistance values by setting the design range α value. Thus, the life of the cells in the proposed module can be increased compared to the operating method that maintains the nominal voltage to be the same as before.

VII. CONCLUSION

This study analyzed the conventional studies on reliability improvement of large-scale ESS applied to railway vehicles and the proposed a new redundant configuration and control method that improves the reliability of the ESS while minimizing system volume increase. In particular, we presented a control method that increased the life of ESSs by controlling the nominal voltage range of newly applied cells (or modules) and aged cells (or modules) differently. Two test battery modules, the conventional type and the proposed type, were manufactured and 14,000-cycle aging tests were conducted using a railway vehicle operating profile. The aging trends of the cells were analyzed by applying various battery aging analysis methods. The analysis results showed that the proposed control method effectively reduced the rate of increase in battery internal resistance, a widely accepted indicator of battery aging. Incremental capacity analysis further validated these results, demonstrating a reduction in aging-related trends. As a result, we confirmed that the life of the battery module can be increased when the proposed control method is applied.

The circuit configuration and the control method proposed in this paper were studied based on the operating profile of railway vehicles, but we expected that it can be applied to various application areas that will require light-weighting of ESSs. In the future, additional research is needed on the control voltage setting method that considers the SOC-internal resistance value table that changes depending on the aging of the cell to enhance the effectiveness of the control method proposed in this paper.

REFERENCES

[1] C. Cambini, R. Congiu, T. Jamasb, M. Llorca, and G. Soroush, "Energy systems integration: Implications for public policy," *Energy Policy*, vol. 143, Aug. 2020, Art. no. 111609.
[2] L. Kavanagh, J. Keohane, G. Garcia Cabellos, A. Lloyd, and J. Cleary, "Global lithium sources—Industrial use and future in the electric vehicle industry: A review," *Resources*, vol. 7, no. 3, p. 57, Sep. 2018.
[3] J. A. Aguado, A. J. S. Racero, and S. de la Torre, "Optimal operation of electric railways with renewable energy and electric storage systems," *IEEE Trans. Smart Grid*, vol. 9, no. 2, pp. 993–1001, Mar. 2018.
[4] Y. M. Ding, S. H. Hong, and X. H. Li, "A demand response energy management scheme for industrial facilities in smart grid," *IEEE Trans. Ind. Informat.*, vol. 10, no. 4, pp. 2257–2269, Nov. 2014.
[5] M. Steiner, M. Klohr, and S. Pagiela, "Energy storage system with ultracaps on board of railway vehicles," in *Proc. Eur. Conf. Power Electron. Appl.*, Aalborg, Denmark, 2007, pp. 1–10.
[6] N. Padmanabhan, M. Ahmed, and K. Bhattacharya, "Battery energy storage systems in energy and reserve markets," *IEEE Trans. Power Syst.*, vol. 35, no. 1, pp. 215–226, Jan. 2020.
[7] N. N. Yazvinskaya, N. E. Galushkin, D. N. Galushkin, and I. A. Galushkina, "Study of effect of batteries capacity on probability of thermal runaway occurrence," *Int. J. Electrochem. Sci.*, vol. 11, no. 10, pp. 8163–8168, Oct. 2016.
[8] N. Mukherjee and D. Strickland, "Second life battery energy storage systems: Converter topology and redundancy selection," in *Proc. 7th IET Int. Conf. Power Electron., Mach. Drives (PEMD)*, Apr. 2014, pp. 1–6.
[9] L. Maharjan, T. Yamagishi, H. Akagi, and J. Asakura, "Fault-tolerant operation of a battery-energy-storage system based on a multilevel cascade PWM converter with star configuration," *IEEE Trans. Power Electron.*, vol. 25, no. 9, pp. 2386–2396, Sep. 2010.
[10] W. Zhang, D. Xu, P. N. Enjeti, H. Li, J. T. Hawke, and H. S. Krishnamoorthy, "Survey on fault-tolerant techniques for power electronic converters," *IEEE Trans. Power Electron.*, vol. 29, no. 12, pp. 6319–6331, Dec. 2014.
[11] F. Chen, W. Qiao, and L. Qu, "A modular and reconfigurable battery system," in *Proc. IEEE Appl. Power Electron. Conf. Expo. (APEC)*, Tampa, FL, USA, Mar. 2017, pp. 2131–2135.

[12] T. Kim, W. Qiao, and L. Qu, "Series-connected self-reconfigurable multicell battery," in *Proc. 26th Annu. IEEE Appl. Power Electron. Conf. Expo. (APEC)*, Fort Worth, TX, USA, Mar. 2011, pp. 1382–1387.
[13] A. Manenti, A. Abba, A. Merati, S. M. Savaresi, and A. Geraci, "A new BMS architecture based on cell redundancy," *IEEE Trans. Ind. Electron.*, vol. 58, no. 9, pp. 4314–4322, Sep. 2011.
[14] S. Muhammad, M. Rafique, S. Li, Z. Shao, Q. Wang, and X. Liu, "Reconfigurable battery systems," *ACM Trans. Des. Autom. Electron. Syst.*, vol. 24, no. 2, pp. 1–27, Mar. 2019.
[15] T. Kim, W. Qiao, and L. Qu, "Power electronics-enabled self-X multicell batteries: A design toward smart batteries," *IEEE Trans. Power Electron.*, vol. 27, no. 11, pp. 4723–4733, Nov. 2012.
[16] T. Zimmermann, P. Keil, M. Hofmann, M. F. Horsche, S. Pichlmaier, and A. Jossen, "Review of system topologies for hybrid electrical energy storage systems," *J. Energy Storage*, vol. 8, pp. 78–90, Nov. 2016.
[17] I.-H. Cho, "Reliability-ensuring configuration for battery-packs of railway vehicles," *J. Korean Soc. Railway*, vol. 26, no. 1, pp. 11–22, Jan. 2023.
[18] G. Yan, D. Liu, J. Li, and G. Mu, "A cost accounting method of the Li-ion battery energy storage system for frequency regulation considering the effect of life degradation," *Protection Control Modern Power Syst.*, vol. 3, no. 1, pp. 1–9, Dec. 2018.
[19] I.-H. Cho, P.-Y. Lee, and J.-H. Kim, "Analysis of the effect of the variable charging current control method on cycle life of Li-ion batteries," *Energies*, vol. 12, no. 15, p. 3023, Aug. 2019.
[20] C. Wu, C. Zhu, Y. Ge, and Y. Zhao, "A review on fault mechanism and diagnosis approach for Li-ion batteries," *J. Nanomaterials*, vol. 2015, no. 1, pp. 1–9, Jan. 2015.
[21] D. Belov and M.-H. Yang, "Failure mechanism of Li-ion battery at overcharge conditions," *J. Solid State Electrochemistry*, vol. 12, nos. 7–8, pp. 885–894, Nov. 2007.
[22] M. Abbas, I. Cho, and J. Kim, "Reliability-constrained optimal sizing and rechargeable battery selection for improved load distribution in a fuel-cell hybrid railway propulsion system," *Energy Convers. Manage.*, vol. 196, pp. 1167–1179, Sep. 2019.
[23] I.-H. Cho, B.-H. Lee, S.-Y. Park, J.-H. Ryu, and J.-H. Kim, "Designing high-voltage and large-capacity battery packs for fuel-cell hybrid railroad propulsion system," *Electronics*, vol. 9, no. 8, p. 1259, Aug. 2020.
[24] C. Pastor-Fernández, K. Uddin, G. H. Chouchelamane, W. D. Widanage, and J. Marco, "A comparison between electrochemical impedance spectroscopy and incremental capacity-differential voltage as Li-ion diagnostic techniques to identify and quantify the effects of degradation modes within battery management systems," *J. Power Sources*, vol. 360, pp. 301–318, Aug. 2017.
[25] S. Y. Park, P. Y. Lee, K. S. Yoo, and J. H. Kim, "A SOH estimation study on lithium-ion battery based on incremental capacity and differential voltage analysis," *Trans. Korean Soc. Mech. Eng. A*, vol. 45, no. 3, pp. 259–266, Mar. 2021.

IN-HO CHO (Member, IEEE) received the master's and Ph.D. degrees in electrical and electronic engineering from Korea Advanced Institute of Science and Technology (KAIST), in 2009 and 2013, respectively. He is currently working as an Associate Professor with the Department of Electrical Engineering, Korea National University of Transportation. His research interests include dc–dc converters, railway vehicle power conversion systems, and battery management systems. He is a member of Korean Institute of Power Electronics and Korea Society for Railway.

SEONG-YUN PARK received the bachelor's degree in mechatronics engineering from Korea University of Technology and Education, in 2016. He is currently working as a Research Engineer with the Energy Storage System Battery Division, LG Energy Solution, Daejeon, Republic of Korea. His current research interests include battery management system (SOx estimation, prediction algorithms, equalization, and screening) and energy storage systems.

BEOM-JUN KIM received the bachelor's degree in electrical engineering from Korea National University of Transportation, in 2023. He is currently pursuing the master's degree with the Power Conversion System Laboratory, Department of Electrical Engineering.

His current research interests include efficient operation of energy systems, battery state estimation, and battery life assessment.

JONG-HOON KIM (Senior Member, IEEE) received the B.S. degree from Chungnam National University, Daejeon, South Korea, in 2005, and the Ph.D. degree in electrical engineering and computer science from Seoul National University, Seoul, South Korea, in 2012. From 2012 to 2013, he was a Senior Research Engineer at the Energy Storage System Development Group, Energy Solution Division, and Samsung SDI, Cheonnan, South Korea. From 2013 to 2016, he was an Assistant Professor at the Department of Electrical Engineering, Chosun University, Gwangju, South Korea. Since 2016, he has been an Associate Professor with the Department of Electrical Engineering, Chungnam National University. Since 2018, he has been an Adjunct Professor with the Eco-Friendly Smart Car Research Center, Korea Advanced Institute of Science and Technology, Daejeon. His research interests include battery management system (SOx estimation, prediction algorithms, equalization, and screening), energy storage systems, and fuel cell systems.